

## Correlation of histopathology with magnetic resonance imaging in Kienbock disease.

著者別名	小川 健, 西浦 康正, 原 友紀, 岡本 嘉一, 落合 直之
journal or publication title	The journal of hand surgery
volume	37
number	1
page range	83-89
year	2012-01
権利	(C) 2012 American Society for Surgery of the Hand. Published by Elsevier Inc. NOTICE: this is the author's version of a work that was accepted for publication in The journal of hand surgery. Changes resulting from the publishing process, such as peer review, editing, corrections, structural formatting, and other quality control mechanisms may not be reflected in this document. Changes may have been made to this work since it was submitted for publication. A definitive version was subsequently published in PUBLICATION, 37, 1, (2012) DOI;10.1016/j.jhsa.2011.09.027
URL	<a href="http://hdl.handle.net/2241/115335">http://hdl.handle.net/2241/115335</a>

doi: 10.1016/j.jhsa.2011.09.027

1 **Correlation of histopathology with magnetic resonance imaging in Kienböck disease**

2  
3 \*Takeshi Ogawa M.D., Ph.D., \*\*Yasumasa Nishiura M.D., Ph.D., \*\*Yuki Hara M.D.,  
4 Ph.D., \*\*\*Yoshikazu Okamoto M.D., Ph.D., \*\*Naoyuki Ochiai M.D., Ph.D.

5  
6 \* Department of Orthopaedic Surgery, Kikkoman general hospital, 100 Miyazaki, Noda,  
7 Chiba, 278-0005, Japan

8 \*\*Department of Orthopaedic Surgery, Graduate School of Comprehensive Human  
9 Sciences, University of Tsukuba, 1-1-1 Tennodai, Tsukuba, Ibaraki, 305-8575, Japan

10 \*\*\* Department of Radiology, Graduate School of Comprehensive Human Sciences,  
11 University of Tsukuba, 1-1-1 Tennodai, Tsukuba, Ibaraki, 305-8575, Japan

12  
13 *Corresponding author:* Takeshi Ogawa, M.D. Ph.D.

14 Department of Orthopaedic Surgery, Kikkoman general hospital, 100 Miyazaki,  
15 Noda-shi, Chiba 278-0005, Japan

16 Tel: +81-4-7123-5911. Fax: +81-4-7123-5920.

17 E-mail address: oga-take@pg7.so-net.ne.jp

18 **【A running title】**

19 Correlation of histopathology with MRI in Kienböck disease

20 **【Key words】**

21 Kienböck disease, histopathology, magnetic resonance imaging, lunate, bone necrosis

22 **【Acknowledgement】**

23 The authors thank Masayuki Noguchi, M.D., Ph.D. (Department of Pathology, Institute  
24 of Basic Medical Science, Graduate School of Comprehensive Human Science,  
25 University of Tsukuba, Tsukuba, Ibaraki, Japan) for the technical assistance and good  
26 advice for pathology.

27

## 28 **Introduction**

29 The treatment of Kienböck disease remains controversial; however, it is agreed that  
30 early diagnosis is important.<sup>1-3</sup> Magnetic resonance imaging (MRI) of Kienböck disease  
31 typically gives a uniformly low signal on T1-weighted images. MRI is essential for an  
32 early diagnosis.<sup>4, 5</sup> However, it is difficult to understand the detail of the actual histology,  
33 which can enable the selection of appropriate treatment options. Few reports have  
34 correlated MRI scans and histopathological appearances of biopsy specimens<sup>6, 7</sup> or  
35 comparisons with sagittal sections of whole lunate bones.<sup>8</sup> As compared to the  
36 histological findings, low-intensity areas on MRI did not correlate closely with the  
37 extent of the necrotic areas and did not distinguish between new bone formation and  
38 granulation tissue. Moreover, Hashizume et al. said that this disagreement was due to  
39 the poor quality of the MRI.<sup>8</sup> Schmitt et al. summarized the pathoanatomic processes  
40 and the corresponding MRI findings in the natural course of lunate osteonecrosis.<sup>9</sup> In  
41 close correlation with the underlying pathoanatomic processes, 3 different signal and  
42 contrast enhancement patterns can be identified in lunate osteonecrosis with the use of  
43 contrast-enhanced, T1-weighted MRI. This imaging technique clearly shows the  
44 different enhancement patterns and differentiation between bone marrow edema and  
45 partial and complete bone marrow necrosis.<sup>9,10</sup>

46 The purpose of this study was to compare in the detail pre-surgery MRI scans with the  
47 corresponding coronal sections of extirpated lunates of patients with Kienböck disease.  
48 Our hypothesis is that the MRI scans taken with 47-mm microscopy surface coil are  
49 reflected the histopathology of Kienböck disease.

## 50 **Materials and methods**

51 Six patients (3 men and 3 women; aged 21–64 years; average 38 years) with Kienböck

52 disease underwent tendon-ball replacement<sup>11</sup> or the Graner surgical procedure (lunate  
53 excision, capitate osteotomy, and intercarpal arthrodesis)<sup>12,13</sup> between 2005 and 2008 at  
54 our Hospital. Each patient was examined by radiography and MRI. Lichtman's criteria  
55 were used to identify stage 3b Kienböck disease on the x-ray.

56 MRI was performed within 1 month before surgery using a 1.5-T system (Gyrosan NT  
57 Intera; Phillips Medical Systems, Best, The Netherlands). Coronal 2-dimensional  
58 proton-density weighted (PDW) ( T1-weighted) (repetition time [TR][msec]/echo time  
59 [TE][msec] = 1697-1852/17.0) images, and fast-field echo (FFE)( T2-weighted) (TR/TE  
60 = 392-396/13.8-14.0) images of the wrist were acquired using a 47-mm microscopy  
61 surface coil (Philips Medical Systems, Best, The Netherlands). The microscopy coil is  
62 intended for a range of applications requiring a small field of view while maintaining a  
63 high signal-to-noise ratio and is well suited to examine small anatomical lesions. The slice  
64 thickness was 1.5-mm, and the slice interval was 0.1-mm with a field of view of  
65 50-mm.<sup>14,15</sup> Under these conditions, the lunate bones were imaged in 8 slices of the  
66 coronal view. A radiologist (Y.O.) and the author (T.O.) observed all preparations and  
67 evaluated the images.

68 The whole lunate bones were extirpated during replacement surgery and were fixed in  
69 a 10% buffered neutral formalin solution (Wako®, Osaka, Japan). After decalcification  
70 in 0.5 M EDTA, 0.1 M Tris and NaOH for 4 months, the samples were embedded in  
71 paraffin. The decalcified whole lunates were sectioned roughly into 8 coronal specimens  
72 (Fig. 1) correlating with the coronal MRI and were stained with hematoxylin-eosin.  
73 Given that a long axis of the lunate was about 20mm, the width of 8 coronal specimens  
74 was about 2mm. Since the slice thickness of MRI was 1.5mm, the error was presumed to  
75 be up to about 1mm.

76 Assessment points of histopathological osteonecrosis included observations of empty  
77 lacunae, fatty marrow, and vascular structures, and the findings were compared with  
78 the signal levels of the PDW- and FFE-coronal MRI at the same slice levels. The author  
79 (T.O.) and another researcher (Y.H.) familiar with histopathological evaluations made  
80 the histological observations of the slices. In total, 8 views from the MRI and 8 slices of  
81 the histopathological specimens that were similar in shape macroscopically were  
82 compared by the author (T.O.) with regards to the assessment points of  
83 histopathological osteonecrosis.

84

## 85 **Results**

86 Generally, PDW images of normal lunates exhibit high signal intensities, whereas FFE  
87 images exhibit intermediate intensities.<sup>7</sup> In comparison, the PDW images of the necrotic  
88 lunate in this study demonstrated lower signal intensities, and the FFE images  
89 exhibited higher or lower intensities.<sup>16</sup> The overall MRI and histopathological  
90 observations of each diseased lunate are shown in Table 1. Sagittal diagrams include  
91 images taken from the central part of the coronal view (Fig. 2). Histopathological  
92 analyses revealed disrupted trabecular and degraded fatty marrows towards the center  
93 of the lunates. However, on the dorsal and palmar aspects of the lunates, the trabecular  
94 structures, fatty marrows, and blood vessels appeared normal. Likewise, the palmar  
95 and dorsal aspects of the lunates maintained near-normal intensities as observed in the  
96 PDW images.

97 The pre-surgical MRI and histopathological images of a representative case are shown  
98 Figure 3. Towards the center of the lunate, the signal intensity of the PDW images was  
99 reduced, and segmented trabecular structures were observed in the corresponding

100 histopathological views. The details of a representative slice level are shown (Fig. 3c, k,  
101 s). Within the solid outline (Fig. 4, upper row), the region appeared nearly normal  
102 histopathologically because we could observe trabecular structures and fatty marrow  
103 (Fig. 4a). This region also exhibited high intensity PDW images and moderate intensity  
104 FFE images. Furthermore, the observed signal was equal to the signal of the normal  
105 osseous tissue in the MRI. Conversely, within the dotted outline (Fig. 4, upper row), the  
106 region was filled with fibrous granular tissue and blood vessels, and no fatty marrow or  
107 osteocyte nuclei were observed histopathologically (Fig. 4b). This region also exhibited  
108 slightly low intensity PDW images and high intensity FFE images. In all specimens, we  
109 observed a signal change on the MRI, as well as changes in the histopathology. In the  
110 dorsal distal region (Fig. 3a, i, q), near-normal signal intensities were observed on the  
111 MRI, and normal trabecular structures were observed in the histopathological analyses,  
112 including osteocyte nuclei, fatty marrow, and blood vessels. This region also exhibited  
113 high intensity PDW images and intermediate intensity FFE images (Fig. 3a, i, q). In the  
114 volar 1/3 area (Fig. 3f, n, v) of the lunate, there were fibrous granular tissues and blood  
115 vessels but an absence of fatty marrow, and this area exhibited low intensity PDW  
116 images and high intensity FFE images.

117 Of the 6 patients having Kienböck disease (stage 3b), osteocyte nuclei, fatty marrow,  
118 and blood vessels were present within the corresponding high intensity areas of the  
119 PDW images. In the low intensity areas of the PDWs, osteocyte nuclei and fatty marrow  
120 were absent, and blood vessels were only present in some of the histopathological  
121 findings. The intensities of the FFE images and the histopathological findings did not  
122 always correlate (Table 2).

123

124 **Discussion**

125 In normal bone, T1-weighted MRI images have a high signal, and T2-weighted MRI  
126 images show an intermediate signal. However, in the early stages of osteonecrosis,  
127 T1-weighted images exhibit a low signal, and T2-weighted images show a high signal.  
128 This intensity change reflects a loss of fatty marrow affecting the T1 signal and possible  
129 edema contributing to a high signal in the T2-weighted images. In the more advanced  
130 stages of osteonecrosis, T1- and T2-weighted images both show low signal intensities.<sup>16</sup>  
131 In the present cases, the lunate conditions were assumed to be advanced osteonecrosis  
132 because of stage 3b on x-ray; however, the MRI scans using a 47-mm microscopy coil  
133 showed a variety of focal changes.

134 Desser et al. (1990) showed that MRI was able to distinguish areas of viable and  
135 nonviable bone within the lunate. They further demonstrated that undecalcified,  
136 fluorescently-labeled histological sections of lunate biopsies exhibited tetracycline  
137 uptake.<sup>7</sup> Trumble et al. (1990) showed that 6 patients having a diagnosis of Kienböck  
138 disease demonstrated a correlation between the loss of signal intensity on T1- and  
139 T2-weighted MRI images and evidence of osteonecrosis by histology. However, the  
140 extent of marrow changes that must be present for signal intensity alterations in MRI  
141 scans has not been determined.<sup>6</sup> Hashizume et al. (1996) histologically examined  
142 extracted whole lunates from 10 patients with Kienböck disease (stage 3). All of the  
143 patients showed a markedly decreased intensity of the lunate on MRI in sagittal  
144 T1-weighted images. In T2-weighted images, 2 cases showed complete low intensity,  
145 and 3 cases yielded diffuse images that included mixed high and low areas. MRI (T1-  
146 and T2-weighted images) low-intensity areas did not correlate closely with the extent of  
147 the necrotic areas in the histological findings and did not distinguish between new bone

148 formation and granulation tissue in detail. Moreover, they said that this disagreement  
149 was due to the poor quality of the MR images.<sup>8</sup> In our 6 cases, empty lacunae and a  
150 reduction of fatty marrow, but not the presence of blood vessels, correlated with the  
151 signal intensities of the PDW images taken with a 47-mm microscopy coil.

152 Kienböck disease is denoted as an avascular necrosis because blood vessels are usually  
153 not present. In the lunates of our study, the trabecular bone structures were segmented,  
154 and fatty marrows were absent, which potentially allowed the formation of fibrous  
155 granulation tissues, although with the presence of blood vessels. Hashizume et al.  
156 (1996) reported that necrotic areas were invaded with new bone formation and  
157 granulation. The necrotic tissue then changed into fibrous scar tissue and necrotic  
158 debris. Around the necrotic area, non-necrotic tissues under hypervascularized  
159 conditions were reactive to the necrosis.<sup>8</sup> Even if there are blood vessels  
160 histopathologically, it is unknown whether there is effective blood flow or interosseous  
161 pressure when evaluated by MRI. If we can know the effective blood flow in the lunate,  
162 it may be useful for selecting treatment or elucidating the etiology of Kienböck disease.

163 Schmitt et al. (2007) classified 3 patterns for Kienböck disease by using  
164 contrast-enhanced MRI and described this classification as the best evaluation for the  
165 viability of bone marrow.<sup>9</sup> Certainly, to evaluate blood flow and the bone marrow edema  
166 of the lunate in detail, gadolinium enhanced MRI is necessary.

167 The absence of gadolinium enhancement in our study is a limitation. Additional  
168 limitations include the small number of cases, low field strength, and minimal imaging  
169 conditions.

170



171 **References**

- 172 1. Beredjikian PK. Kienbock's disease. *J Hand Surg* 2009; 34A:167-175.
- 173 2. Innes L, Strauch RJ. Systematic review of the treatment of Kienbock's disease  
174 in its early and late stages. *J Hand Surg Am* 2010; 35:713-7, 17 e1-4.
- 175 3. Squitieri L, Petruska E, Chung KC. Publication bias in Kienbock's disease:  
176 systematic review. *J Hand Surg Am* 2010; 35:359-367 e5.
- 177 4. Amadio PC, Hanssen A D, Berquist TH. The genesis of Kienbock's disease:  
178 evaluation of a case by magnetic resonance imaging. *J Hand Surg Am* 1987;  
179 12:1044-1049.
- 180 5. Imaeda T, Nakamura R, Miura T, Makino N. Magnetic resonance imaging in  
181 Kienbock's disease. *J Hand Surg Br* 1992; 17:12-19.
- 182 6. Trumble TE, Irving J. Histologic and magnetic resonance imaging correlations  
183 in Kienbock's disease. *J Hand Surg Am* 1990; 15:879-884.
- 184 7. Desser TS, McCarthy S, Trumble T. Scaphoid fractures and Kienbock's disease  
185 of the lunate: MR imaging with histopathologic correlation. *Magn Reson*  
186 *Imaging* 1990; 8:357-361.
- 187 8. Hashizume H, Asahara H, Nishida K, Inoue H, Konishiike T. Histopathology of  
188 Kienbock's disease. Correlation with magnetic resonance and other imaging  
189 techniques. *J Hand Surg Br* 1996; 21:89-93.
- 190 9. Schmitt R, Krimmer H. Osteonecrosis of the hand skeleton. In: Schmitt R,  
191 Lanz U, eds. *Diagnostic Imaging of the Hand*. 1st ed. Stuttgart, New  
192 York: Georg Thieme Verlag; 2007; 351-364.
- 193 10. Schmitt R, Christopoulos G, Kalb K, Coblenz G, Frohner S, Brunner H,  
194 Krimmer H, Lanz U. Differential diagnosis of the signal-compromised lunate in

195 MRI. *Rofo* 2005; 17: 358-366.

196 11. Ueba Y, Nosaka K, Seto Y, Ikeda N, Nakamura T. An operative procedure for  
197 advanced Kienbock's disease. Excision of the lunate and subsequent  
198 replacement with a tendon-ball implant. *J Orthop Sci* 1999; 4:207-215.

199 12. Graner O, Lopes EI, Carvalho BC, Atlas S. Arthrodesis of the carpal bones in  
200 the treatment of Kienbock's disease, painful ununited fractures of the  
201 navicular and lunate bones with avascular necrosis, and old  
202 fracture-dislocations of carpal bones. *J Bone Joint Surg Am* 1966; 48: 767-774.

203 13. Takase K, Imakiire A. Lunate excision, capitate osteotomy, and intercarpal  
204 arthrodesis for advanced Kienbock disease. Long-term follow-up. *J Bone Joint*  
205 *Surg Am* 2001; 83: 177-183.

206 14. Tanaka T, Yoshioka H, Ueno T, Shindo M, Ochiai N. Comparison between  
207 high-resolution MRI with a microscopy coil and arthroscopy in triangular  
208 fibrocartilage complex injury. *J Hand Surg Am* 2006; 31: 1308-1314.

209 15. Yoshioka H, Ueno T, Tanaka T, Kujiraoka Y, Shindo M, Takahashi N, Nishiura  
210 Y, Ochiai N, Saida Y. High-resolution MR imaging of the elbow using a  
211 microscopy surface coil and a clinical 1.5 T MR machine: preliminary results.  
212 *Skeletal Radiol* 2004; 33: 265-271.

213 16. Schmitt R, Heinze A, Fellner F, Obletter N, Struhn R, Bautz W. Imaging and  
214 staging of avascular osteonecroses at the wrist and hand. *Eur J Radiol* 1997;  
215 25: 92-103.

216

217 **Figure legends**

218 Figure 1. Whole lunate with a schema of the 8 coronal slices scanned using MRI.

219 Figure 2. MRI analysis of each patient. Sagittal diagrams include images taken from  
220 the central part of the coronal view.

221 Figure 3. Pre-surgical PDW images (a–h) and FFE images (i–p) and HE stained sections  
222 (q–x) (x 12.5) taken from the dorsal to palmar side of the lunate from a 21-year-old  
223 left-handed woman that underwent a Graner surgical procedure for Kienböck disease  
224 (stage 3b).

225 Figure 4. Representative slice levels (taken from Fig. 2c, k, s) and correlating histology.  
226 Within the solid outline (upper row), the region appeared nearly normal  
227 histopathologically because we could observe trabecular structures and fatty marrow (a).  
228 This region also exhibited high intensity PDW images and moderate intensity FFE  
229 images and was equal to the signal of the normal osseous tissue in the MRI. Conversely,  
230 within the dotted outline (upper row), this region contained fibrous granular tissue and  
231 blood vessels, and no fatty marrow or osteocyte nuclei were observed histopathologically  
232 (b). (a) A high magnification image of the squared encircled area in (c, k and s).  
233 Osteocyte nuclei, fatty marrow, and blood vessels are present within the vitalized focal  
234 area of the solid line. (b) Fibrous granular tissues and blood vessels are present,  
235 whereas there is an absence of fatty marrow within the dotted line.

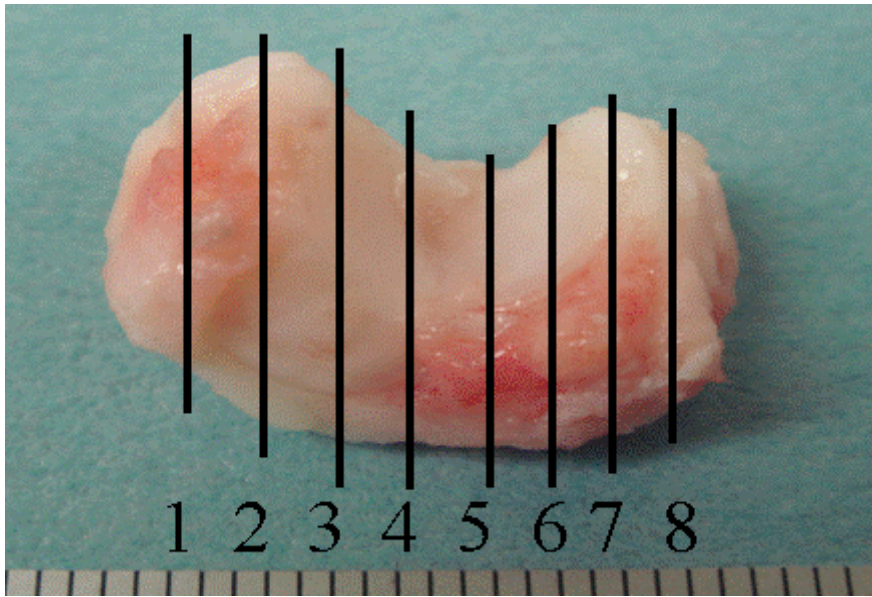
236

237 Table 1. MRI and histopathological analysis of each patient.

238 Table 2. Correlation of the histopathology with the MRI scans: (+), presence; (±),  
239 discordance; (-), absence.

240

241 Figure 1.



242

243

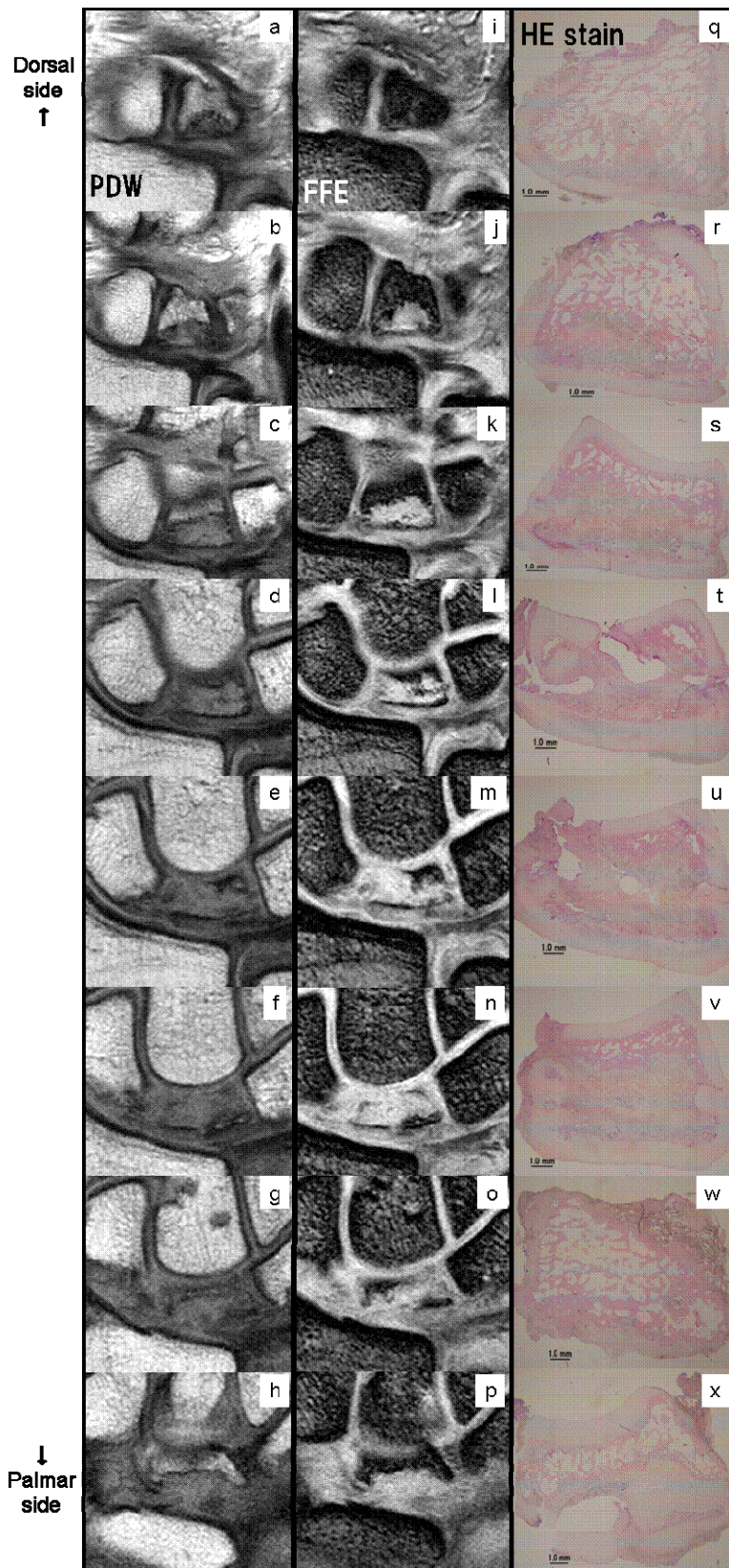
244 Figure 2.

245

246

Patient	MRI finding			
	PDW		FFE	
		sagittal diagram		sagittal diagram
1	normal or partial slightly low (dorsal 1/3 and volar 1/3), low (central 1/3)		normal (dorsal 1/3 and volar 1/4), low (another central part)	
2	normal (dorsal 1/2), low (volar 1/2)		normal (dorsal 1/2), low (volar 1/2)	
3	normal (dorsal 1/4 and volar-ulnar sides), low (dorsal 1/4 to volar-radial sides)		high (dorsal 1/3 and volar-ulnar sides), low (dorsal 1/3 to volar-radial sides)	
4	all slices are slightly low		all slices are high and low (diffuse or partial)	
5	low (volar 1/4), another slices are slightly low		normal (dorsal 1/3), high (diffuse or partial) (center to volar side)	
6	normal or partially slight low (dorsal 1/3 and volar 1/3), low (central 1/3)		high (dorsal 3/4), normal (volar 1/4)	
Normal	hyperintense signal		intermediate signal	

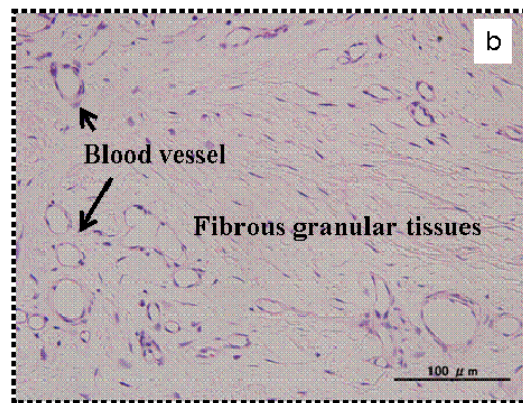
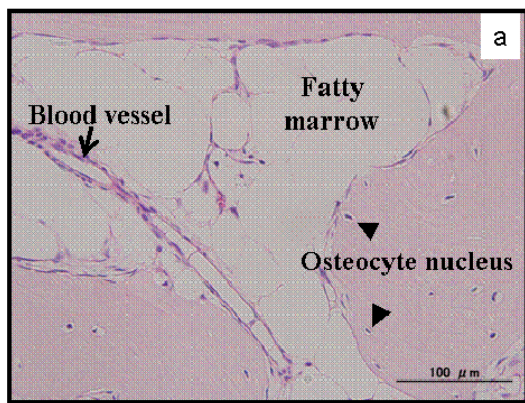
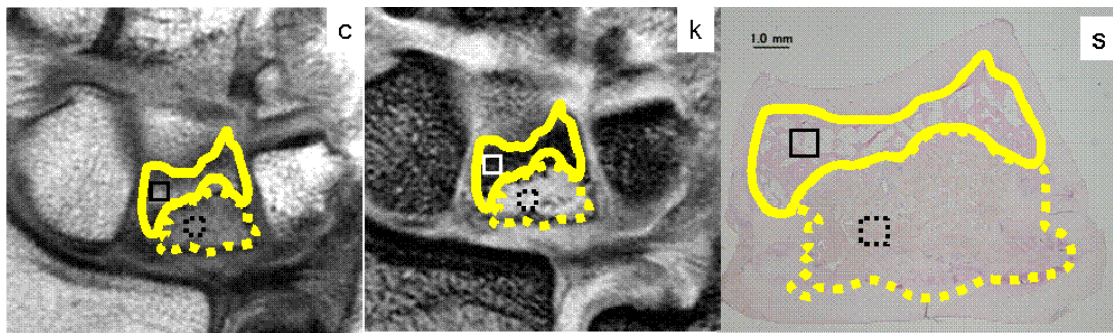
247 Figure 3.



248

249

250 Figure 4.



251

252

253 Table 1.

Patient	Gender	Age	X-ray finding	Histopathological finding			MRI finding	
				Empty lacunae	Fatty marrow	Blood vessel	PDW	FFE
1	F	65	segmentation and comminuted fracture at central 1/3	partially presence (central 1/3), a few (dorsal 1/3 and volar 1/3)	absence (central 1/3), partially presence (dorsal 1/3 and volar 1/3)	partially presence in all slices	normal or partial slightly low (dorsal 1/3 and volar 1/3), low (central 1/3)	normal (dorsal 1/3 and volar 1/4), low (another central part)
2	M	24	segmentation at volar 1/3	presence (dorsal1/3), absence (volar2/3)	presence (dorsal1/3), absence (volar2/3)	presence (dorsal1/3), absence (volar2/3)	normal (dorsal1/2), low (volar1/2)	normal (dorsal1/2), low (volar1/2)
3	M	21	severe collapse, especially radial side	partially presence in all slices	partial presence (dorsal1/4 and volar-ulnar side)	partially presence in all slices	normal (dorsal1/4 and volar-ulnar sides), low(dorsal 1/4 to volar-radial sides)	high (dorsal1/3 and volar-ulnar sides), low (dorsal 1/3 to volar-radial sides)
4	M	33	segmentation(+) coronal and sagittal plane on center	partially presence in all slices	partially presence (dorsal 1/3) , absence (central to volar 1/3)	partially presence in all slices	all slices are slightly low	all slices are high and low (diffuse or partial)
5	F	64	segmentation at volar 1/3	presence (dorsal2/3), absence (volar1/3)	absence in all slices	dorsal2/3 is absence, volar1/3 is presence	low (volar1/4), another slices are slightly low	normal (dorsal 1/3), high(diffuse or partial)(center to volar side)
6	F	21	segmentation and comminuted fracture at volar 1/3	partially presence (central 1/3), a few (dorsal 1/3 and volar 1/3)	absence (central 1/3), partially presence (dorsal 1/3 and volar 1/3)	partially presence in all slices	normal or partially slight low (dorsal 1/3 and volar 1/3), low (central 1/3)	high (dorsal3/4), normal (volar 1/4)
	Normal		sclelotic change (-) collapse (-) segmentation(+)	absence	presence	presence	hyperintense signal	intermediate signal

254

255



256 Table 2.

257

MRI finding		Histopathological finding			osteonecrosis
		Osteocyte nucleus	Fatty marrow	Blood vessel	
PDW image	intermediate	+	+	+	-
	slightly low	-	-	±	+
	low	-	-	±	+
FFE image	high	±	±	±	±
	intermediate	+	+	+	-
	low	±	±	±	±

258

259

260 **Abstract**

261 **Purpose** Diagnosis and treatment remain controversial for Kienböck disease. A few  
262 reports have correlated magnetic resonance imaging (MRI), which is essential for early  
263 diagnosis, and histopathology of Kienböck biopsy specimens, but histopathological  
264 correlations of whole lunate bones or histological slices compared with MRI images are  
265 lacking. The purpose of this study was to compare pre-surgical MRI scans taken with a  
266 47-mm microscopy surface coil with corresponding histological slices of Kienböck  
267 diseased lunates.

268 **Materials and methods** Extirpated whole lunates were harvested at the time of  
269 surgery from 6 patients with Kienböck disease (stage 3b) undergoing tendon-ball  
270 replacement or a Graner surgical procedure. Paraffin-embedded, coronally sectioned  
271 specimens were stained with hematoxylin-eosin and compared with pre-surgical coronal  
272 scans using MRI with a 47-mm microscopy surface coil.

273 **Results** Towards the center of the lunates, the signal intensity in the proton-density  
274 weighted (PDW) images was reduced, whereas the dorsal and palmar sides of the  
275 lunates exhibited no changes in intensity. In correlation, histopathological findings  
276 revealed strongly disrupted trabeculae toward the center of the lunates and intact  
277 trabeculae in the dorsal side of the lunates. Likewise, the necrotic and vitalized bone  
278 exhibited low and high signal intensities, respectively, in the PDW images; however, in  
279 the fast-field echo (FFE) images, there were no correlations with the histopathological  
280 observations.

281 **Conclusions** MRI (PDW images, but not FFE images) using a 47-mm microscopy coil  
282 reflected the extent and localization of the necrotic area in Kienböck diseased lunates,  
283 as evidenced by comparison with histological analyses of the lunate specimens.